Technical Paper by J. Koseki, Y. Munaf, F. Tatsuoka, M. Tateyama, K. Kojima and T. Sato

SHAKING AND TILT TABLE TESTS OF GEOSYNTHETIC-REINFORCED SOIL AND CONVENTIONAL-TYPE RETAINING WALLS

ABSTRACT: A series of shaking table tests was performed on relatively small-scale models of a geosynthetic-reinforced soil retaining wall with a full-height rigid facing and conventional type (gravity-type, leaning-type, and cantilever-type) retaining walls. Tilt table tests were also conducted on the geosynthetic-reinforced soil retaining wall and the leaning-type model walls. The seismic stability of these different types of walls are evaluated by both shaking and tilt table test methods and compared with each other. The observed critical seismic acceleration coefficients are compared with the values predicted by the conventional pseudo-static approach. Similarly, the observed failure plane angles in the backfill are compared with the predicted values. The effects of simple shear deformation of the reinforced backfill for the reinforced-type walls and the effects of post-peak reduction of shear resistance along the failure plane are also discussed.

KEYWORDS: Retaining wall, Model test, Shaking table, Tilt table, Pseudo-Static analysis, Limit equilibrium analysis, Geosynthetic, Earthquake load.

AUTHORS: J. Koseki, Associate Professor, Y. Munaf, Graduate Student, and T. Sato, Research Associate, Institute of Industrial Science, University of Tokyo, 7-22-1 Roppongi, Minato-ku, Tokyo 106-8556, Japan, Telephone: 81/3-3402-6231, Telefax: 81/3-3479-0261, E-mail; koseki@iis.u-tokyo.ac.jp; F. Tatsuoka, Professor, Department of Civil Engineering, University of Tokyo, 7-3-1 Hongo, Bunkyo-ku, Tokyo 113-8656, Japan, Telephone: 81/3-3812-2111, Telefax: 81/3-5689-7268, E-mail; tatsuok@hongo.ecc.u-tokyo.ac.jp; and M. Tateyama and K. Kojima, Railway Technical Research Institute, 2-8-38 Hikari-machi, Kokubunji-shi, Tokyo 185-8540, Japan, Telephone: 81/425-73-7261, Telefax: 81/425-73-7248, E-mail: tate@rtri.or.jp and kojima@soilf.rtri.or.jp.

PUBLICATION: *Geosynthetics International* is published by the Industrial Fabrics Association International, 1801 County Road B West, Roseville, Minnesota 55113-4061, USA, Telephone: 1/612-222-2508, Telefax: 1/612-631-9334. *Geosynthetics International* is registered under ISSN 1072-6349.

DATES: Original manuscript received 9 July 1997, revised version received 18 December 1997 and accepted 2 January 1998. Discussion open until 1 September 1998.

REFERENCE: Koseki, J., Munaf, Y., Tatsuoka, F., Tateyama, M., Kojima, K. and Sato, T., 1998, "Shaking and Tilt Table Tests of Geosynthetic-Reinforced Soil and Conventional-Type Retaining Walls", *Geosynthetics International*, Vol. 5, Nos. 1-2, pp. 73-96.

1 INTRODUCTION

A number of conventional masonry and unreinforced concrete gravity-type retaining walls for railway embankments were seriously damaged by the 1995 Hyogoken-Nanbu earthquake in Japan. Many modern cantilever-type, reinforced concrete (RC) retaining walls were also damaged, while geogrid-reinforced soil retaining walls with a full height RC facing performed well during the earthquake (Tatsuoka et al. 1996a,b).

Pseudo-static limit equilibrium-based stability analyses that follow one of the current aseismic design methods in Japan were conducted by the authors of the current paper on five damaged retaining walls (Koseki et al. 1996). It was found that the critical seismic acceleration coefficient, $k_{h\text{-}cr}$, yielding a factor of safety of unity against external instability (i.e. sliding, overturning, or bearing capacity failure) was approximately 40 to 80% of the estimated peak horizontal ground acceleration, *PHGA*, divided by the gravitational acceleration, *g*, except for one cantilever-type RC retaining wall. This cantilever-type wall was extremely unstable prior to the earthquake due to the existence of an additional upper embankment on the crest behind the wall. Since the values of $k_{h\text{-}cr}/(PHGA/g)$ were almost equal irrespective of the extent of damage (i.e. among the severely damaged gravity-type retaining walls, the moderately damaged cantilever-type RC retaining wall, and the slightly damaged geogrid-reinforced soil retaining wall), it was inferred that the current aseismic design method for these different types of retaining walls are inadequate. Therefore, it is required to compare the seismic performance of different types of retaining walls to establish consistent aseismic design methods.

In Japan, geosynthetic-reinforced soil retaining walls with a full-height RC facing have been constructed to a total length exceeding 26 km as important permanent structures mainly for railways (Tatsuoka et al. 1997). Many of these walls were aseismically designed by using a pseudo-static, limit equilibrium-based stability analysis as described by Horii et al. (1994). Use of these walls will be further promoted when their ductile behavior against earthquake loads, as discussed by Tatsuoka et al. (1996a), is rationally evaluated and taken into account in the aseismic design procedure.

Shaking table tests on small-scale models of geosynthetic-reinforced soil retaining walls were conducted by several other researchers as summarized by Bathurst and Alfaro (1996). However, comparisons of their seismic behavior to that of other types of retaining walls is scarce; Sakaguchi (1996) compared the dynamic stability of a geogrid-reinforced soil retaining model wall having wrapped-around facing with that of model conventional-type (gravity-type, leaning-type, and cantilever-type) retaining walls.

With respect to the seismic behavior of geosynthetic-reinforced soil retaining walls with a full-height rigid facing, Murata et al. (1992, 1994) conducted a series of shaking table tests primarily to investigate the effect of facing rigidity on the resistance capacity against earthquake load. However, no comparison was made with other types of retaining walls. It should also be noted that tilt table tests have not been conducted on model geosynthetic-reinforced soil retaining walls, even though this type of test can simulate pseudo-static loading conditions which are assumed in most of the current aseismic design methods based on the limit equilibrium stability analysis. Furthermore, it can be expected that the comparison of model behavior between shaking table tests and tilt table tests reveals the dynamic effects on wall stability and, it is hoped, any inconsistency between the pseudo-static analysis and the actual seismic behavior.

Considering the above situation, a series of shaking table tests was performed on relatively small-scale models of a geosynthetic-reinforced soil retaining wall with a full-height rigid facing and three types of conventional-type retaining walls (gravity-type, leaning-type, and cantilever-type). Tilt table tests were also conducted on models of a geosynthetic-reinforced soil retaining wall and the leaning-type wall.

The current paper describes the critical accelerations/tilting angles and the angles of the failure plane in the backfill layers that were observed during the experiments. Analyses based on the recorded earth pressures, wall displacements, and response accelerations will be reported elsewhere. These data may reveal important features with respect to the mechanism of mobilization of seismic earth pressure, when comparing the ductile behavior of different types of retaining walls, and when evaluating the dynamic effects which include amplification and phase difference.

2 TESTING PROCEDURE

2.1 The Model Reinforced Sand and Retaining Walls

The cross sections of five different model retaining walls used in this study are shown in Figure 1. The broken lines show the initial locations and the hatched zones show the displaced locations observed after failure of the model retaining wall. The total height of the walls was 530 mm except for the reinforced soil-type wall which was 500 mm high. The width of the base of the cantilever-type and gravity-type walls was 230 mm, and it was reduced to 180 mm for the leaning-type wall. To the measure normal stress, σ, and shear stress, τ, components of the earth pressures acting on the back of the facing and the base of the walls, several two-component load cells were installed (see Figure 2 for the load cell locations in a typical cantilever-type wall). The details of the two-component load cells were described by Tatsuoka et al. (1989). The load cells were located within a 150 mm width along the center line of the wall to alleviate the effects of side wall friction. To form a rigid structural body for the model wall, wooden blocks (used for dummy walls) were stacked on both sides of the center section that was instrumented with load cells and the blocks were reinforced with steel bars.

In conducting static loading tests on similar small-scale model walls, Tatsuoka et al. (1989) lubricated the inside of the sand box by using a sheet of latex membrane smeared with a thin layer of silicone grease. However, this method of lubrication was not employed in this study because it was not expected to be effective for dynamic tests. Instead, the width of the sand box in the direction of the wall facing was enlarged by a factor of 1.5 to 600 mm, the earth pressures were measured at the center line as mentioned in the previous paragraph. To adjust the dead load of the gravity- and leaning-type model walls, extra weights were added near the center of gravity of these walls.

For model the reinforced-soil retaining walls, a grid of phosphor-bronze strips was used as the model reinforcement (Figure 3). Each strip was 3 mm wide and 0.1 mm thick and had a bending stiffness, EI , of approximately 0.003 N-m^2 (Tatsuoka et al. 1989). These materials and dimensions were selected to enable the tensile forces acting on the model reinforcement to be measured, by attaching strain gauges at several locations on the reinforcing strips. To form a lattice-shaped layer of model reinforcement that simulates geogrids in actual field conditions, strips were glued together at 50 mm intervals

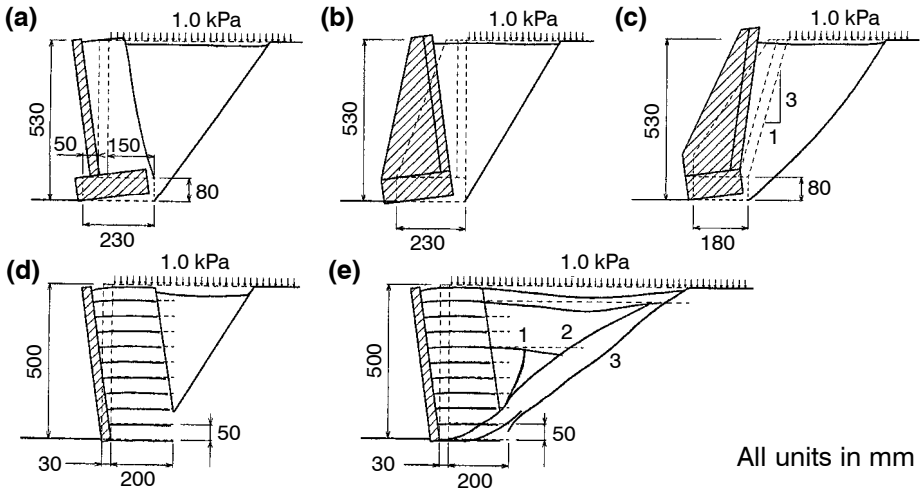

Figure 1. Initial and displaced locations and observed failure planes in the model retaining walls: (a) cantilever-type; (b) gravity-type; (c) leaning-type; (d) reinforced soil, Type 1; (e) reinforced soil, Type 2.

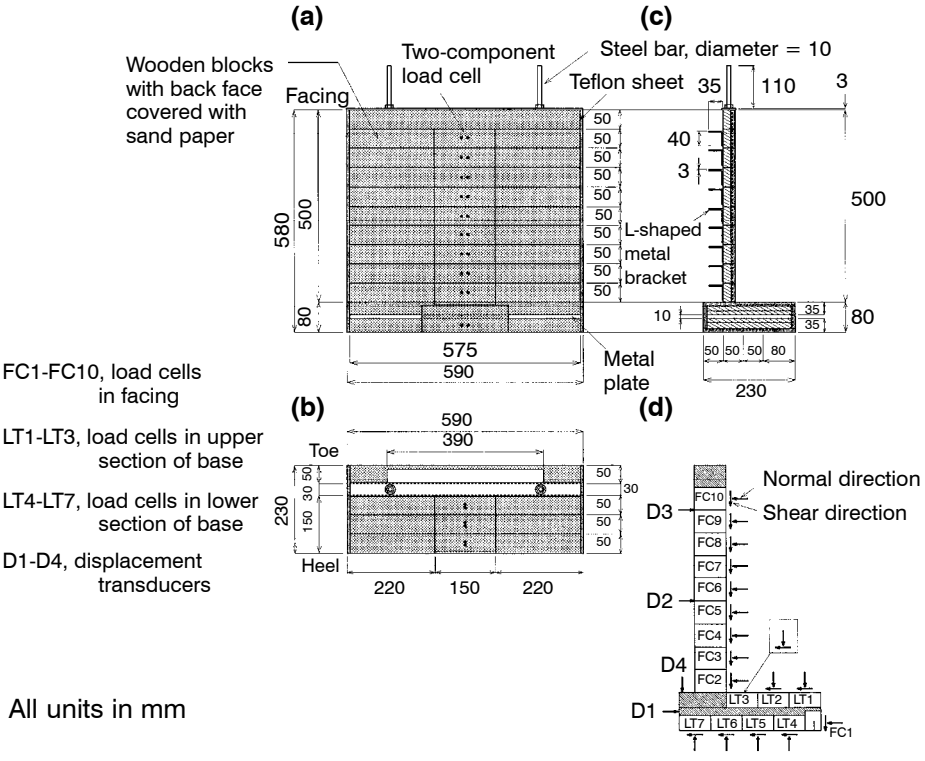

Figure 2. Structural details of the model cantilever-type retaining wall: (a) front view; (b) plan view; (c) side view; (d) load cells installed at the center line.

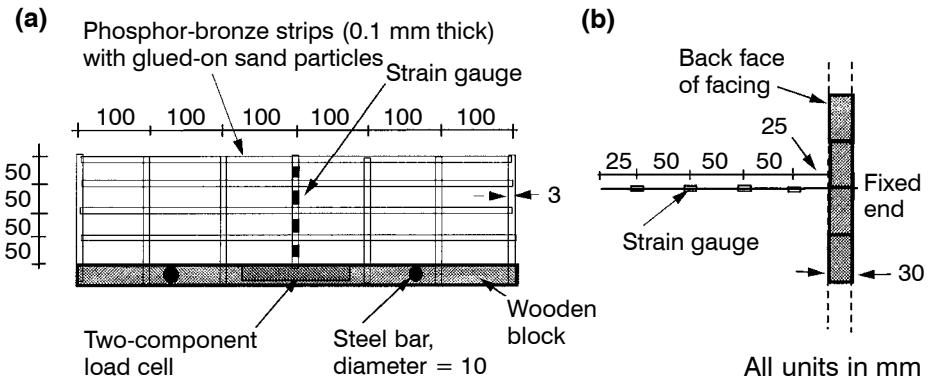

Figure 3. Configuration of the model wall reinforcement: (a) plan view; (b) cross section.

in the direction parallel to the side wall and at 100 mm intervals in the direction normal to the side wall. To mobilize friction between the reinforcement and the backfill soil, as mobilized by actual geogrids, sand particles were glued to the surface of the strips. Ten layers of model reinforcement having a length of 200 mm were used for the reinforced soil, Type 1 model walls. On the other hand, the length of the top and fourth layers were increased to 800 mm and 450 mm, respectively, for the reinforced soil, Type 2 model wall in order to increase the stability against overturning, as is the common practice in Japan. It should be noted that any internal failure mode of the reinforcement, such as a breakage or an excessive elongation, as well as that of the overall wall structure, is not within the scope of the current paper.

A fine, uniformly graded quartz-rich sand having subangular particles (i.e. Toyoura sand, d_{50} = 0.16 mm, e_{max} = 0.997, e_{min} = 0.605) was used as the backfill and subsoil layers. It was pluviated at an air-dried condition by using a sand hopper. The sand box had internal dimensions of 2.6 m long, 0.6 m wide, and 1.4 m high for the shaking table tests (Figure 4), and 2.0 m long, 0.6 m wide, and 0.8 m high for the tilt table tests. To prepare homogeneous dense sand layers at a void ratio of 0.630, the fall height of the sand and the traveling speed of the sand hopper were kept constant at 0.8 m and 0.042 m/s, respectively. To observe the deformation/displacement of the sand layers, horizontal layers of black, dyed Toyoura sand having a thickness of 10 mm were prepared at a vertical spacing of 50 mm.

For all of the model walls, sand paper was glued to the surface of the load cells and the wooden blocks that were in contact with the backfill and the subsoil layers, in order to mobilize friction.

The configurations of the model walls used in the shaking table tests, and test results are summarized in Table 1. To prepare each model for the shaking table tests, a subsoil layer with a thickness of 200 mm was pluviated, the model wall was carefully installed, backfill layers were pluviated, and then a surcharge of 1.0 kPa consisting of lead shots equally placed on the top of the backfill layers in order to simulate a prototype surcharge was applied. It should be noted that for one of the reinforced soil, Type 1 model walls used in the tilt table tests, the amount of the surcharge was increased to 3.1 kPa in order

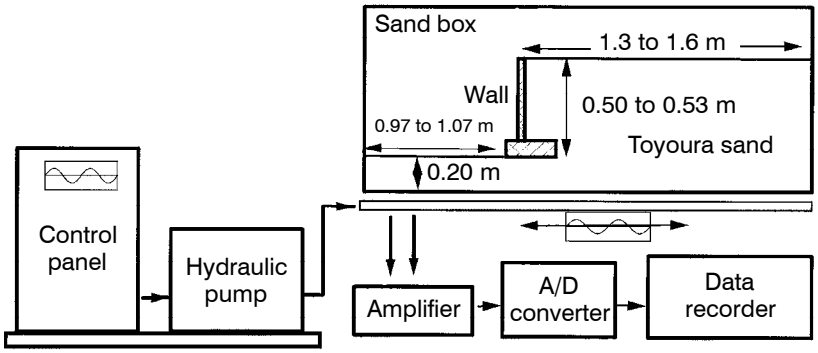

Figure 4. The excitation and data acquisition systems for the shaking table tests.

to evaluate the effects of a different surcharge. The surcharge increases the stress level in the backfill, which helps to measure earth pressures with higher resolution and reduces the relative effect of side wall friction. The model walls, excluding those of the reinforced soil-type, were not propped in order to move freely during the preparation stages. The earth pressures in the soil layers, displacement of the wall, and the tilting angle of the sand box were recorded. For the reinforced soil-type model walls, the horizontal displacement was constrained by propping the wall during pluviation of the backfill sand to avoid excessive movement, and the constraint was released after the backfill layers and the surcharge were completed.

Table 1. The model walls used in the shaking table tests.

Model	Wall type	Surcharge on backfill (kPa)	Observed critical acceleration (gal)	Angle of the failure plane, ζ, observed at the end of test* (°)
S-2	Cantilever	1.0	430	55
S-3	Gravity	1.0	398	59
S-4	Leaning	1.0	301	51
S-5	Leaning	1.0	334	50
S-6	Leaning	1.0	319	49
S-7	Reinforced soil 1	1.0	529	58
S-8	Reinforced soil 2	1.0	654	70, 53, 40

Notes: * Refer to Figure 10 for the definition of ζ. The values indicated for the reinforced soil, Type 2 wall are, respectively, for the 1st, 2nd, and 3rd failure plane (refer to Figure 1), which were not corrected for the wall configuration before deformation.

2.2 Shaking Table Tests

After model preparation, the sand box was subjected to horizontal sinusoidal shaking at a frequency of 5 Hz. For the cantilever-type model wall, the amplitude of the base acceleration was initially set to approximately 25 gals (the gravitational acceleration is equal to approximately 981 gals) and was increased at an increment of approximately 25 gals. For the other models, however, the initial base acceleration was initially set to approximately 50 gals, and the increment was doubled to approximately 50 gals in order to reduce the possible effects of the previous shaking history on the wall behavior during the subsequent loading stages.

In the current paper, the effects of these two different time histories of shaking table acceleration on the test results were assumed to be insignificant. At each acceleration level, the same amplitude was maintained for approximately 10 seconds. Shaking was terminated when the wall displacement became considerably large and was restricted by locking devices set to prevent a complete collapse of the wall. Response accelerations of both the wall and the backfill layers were recorded, as well as the wall displacement, the earth pressures in the soil layers, and the tensile forces in the reinforcement. Figure 5 shows the locations of displacement transducers, accelerometers, and earth pressure cells in the model walls used for the shaking table tests. Typical shaking table test results for the reinforced soil, Type 1 model wall are shown in Figures 6 and 7.

2.3 Tilt Table Tests

Three tilt table tests were performed and are summarized in Table 2. After preparation of the models in a rigid sand box, which was similar to that of the shaking table tests, the whole sand box was tilted, as schematically shown in Figure 8, at a continuous rate of approximately 1.0 °/minute until considerable displacement of the wall was observed.

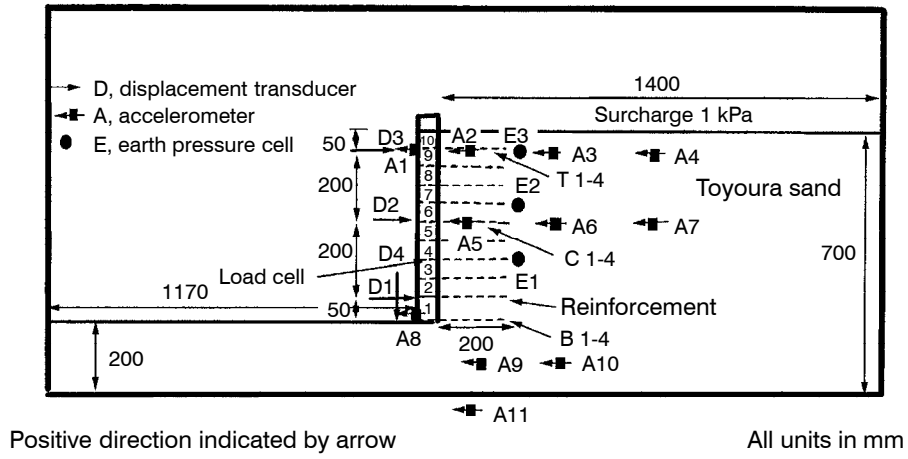

Figure 5. Location of instrumentation in the model reinforced soil, Type 1 walls for the shaking table tests.
Note: T, C, and B = top, center, and bottom reinforcement locations, respectively.

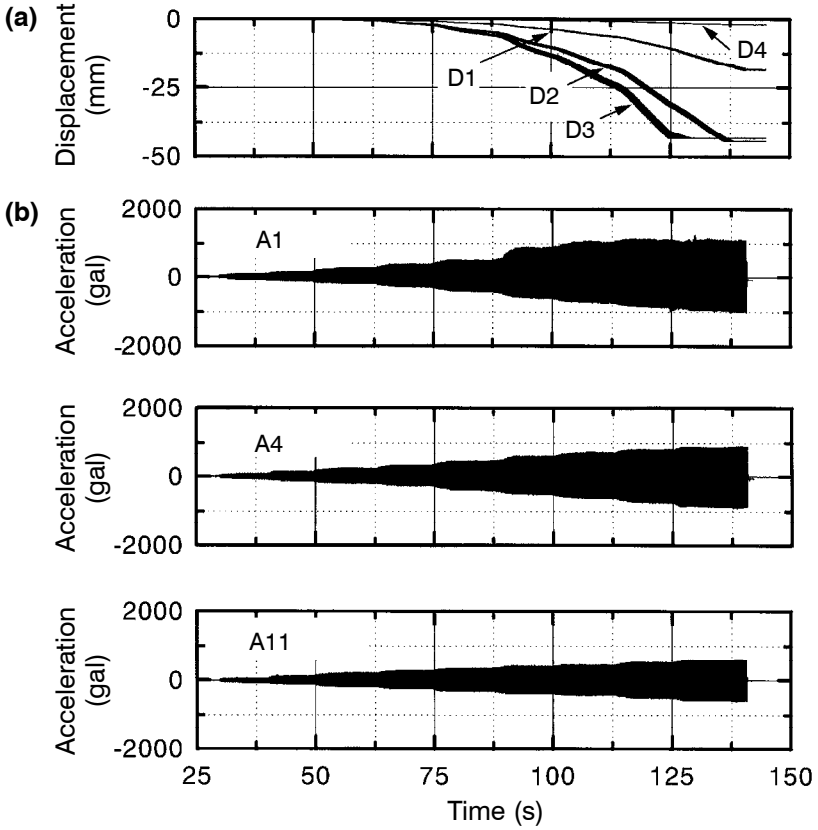

Figure 6. Typical recorded data for a reinforced soil, Type 1 retaining model wall during shaking table tests: (a) displacement; (b) acceleration time histories.

Note: See Figure 5 for the location of accelerometers, A1, A4, and A11, and for the location of displacement transducers, D1 to D4. 1gal = 0.001g.

Table 2. A summary of the model wall tilt table test results.

Model designation	Type of model wall	Surcharge at backfill (kPa)	Tilting angle, θ, at failure (°)	Angle of failure plane, ζ, observed at the end of test (°)*
T-8	Leaning	1.0	11.3	51
T-9	Reinforced soil 1	3.1	16.3	56
T-11	Reinforced soil 1	1.0	20.6	56

Notes: * Refer to Figure 10 for the definition of ζ and to Figure 8 for the definition of θ.

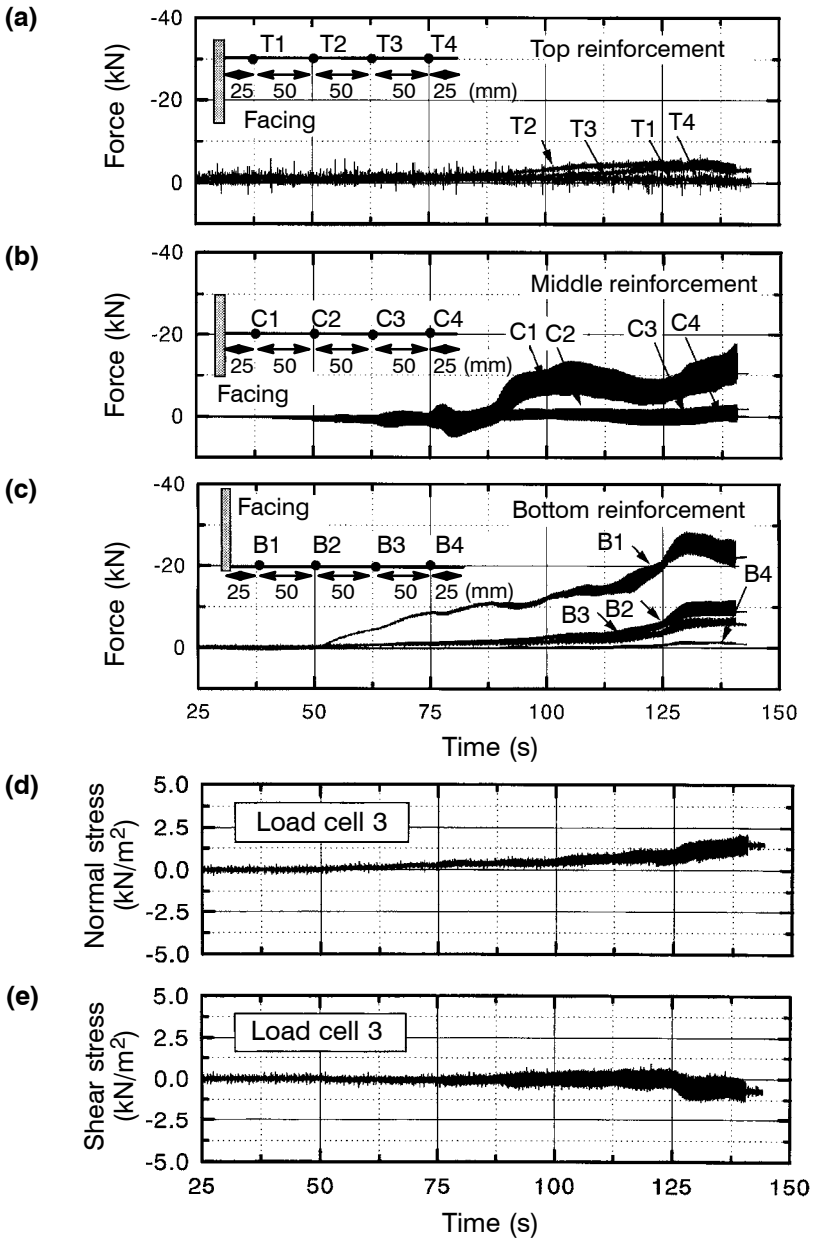

Figure 7. Typical recorded data for a reinforced soil, Type 1 retaining model wall during shaking table tests: (a) forces measured in the top layer of reinforcement; (b) forces measured in the middle layer of reinforcement; (c) forces measured in the bottom layer of reinforcement; (d) normal stress; (e) shear stress.

Note: See Figure 5 for the locations of T1 to T4, C1 to C4, B1 to B4, and load cell 3 which is located at the lower part of the facing.

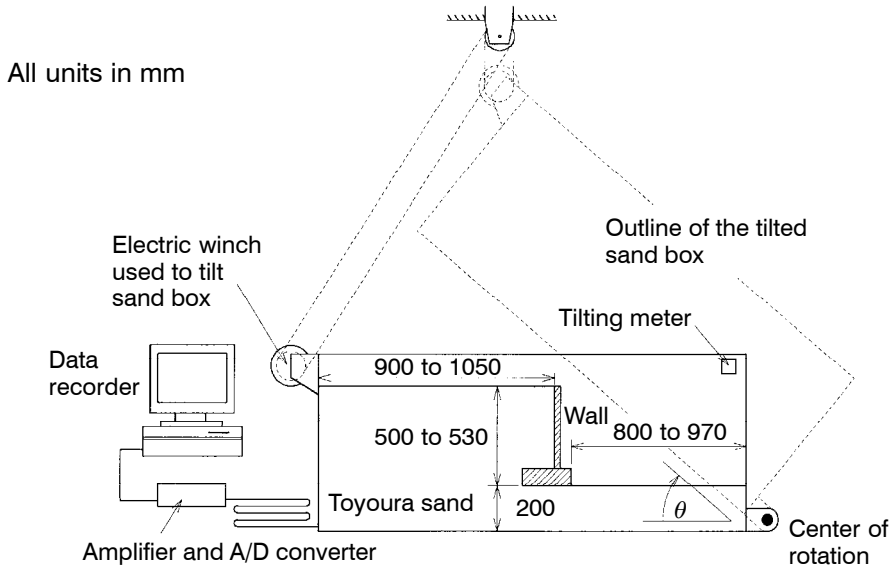

Figure 8. Tilt table test procedure, and the definition of the tilting angle, θ.

3 EVALUATION OF WALL STABILITY BASED ON THE PSEUDO-STATIC APPROACH

Factors of safety against overturning and sliding of tilted model walls were evaluated based on a pseudo-static approach. The backfill earth pressures were estimated using the two-wedge method for the reinforced soil-type wall, as described by Horii et al. (1994) (Figure 9), and the Mononobe-Okabe method (using a single wedge) for the other types of model walls. In both methods, earth pressures due to the self-weight of the backfill were assumed to be hydrostatically distributed, and those due to the surcharge at the top of the backfill were assumed to be uniformly distributed.

It should be noted that in previous studies (e.g. Bathurst and Cai 1995), a dynamic increment of the earth pressures was assumed to have a higher point of application than the hydrostatic distribution. In this study, however, the assumption of a hydrostatic distribution was employed because it was broadly used in the current, aseismic design practice for retaining walls in Japan.

Based on the plane strain compression test results for the Toyoura sand which was used in the model tests, at a low confining pressure (9.8 kPa) the shear resistance angle, ϕ, of the backfill and subsoil layers was evaluated to be 51° when the major principal stress, σ_1, direction was vertical. For the cantilever-type wall, having a wall base underlain by the backfill, a virtually vertical back face was assumed within the backfill as shown in Figure 10. The portion of the backfill located above the wall base and between the back of facing and the virtually vertical back face was regarded to be a part of the wall.

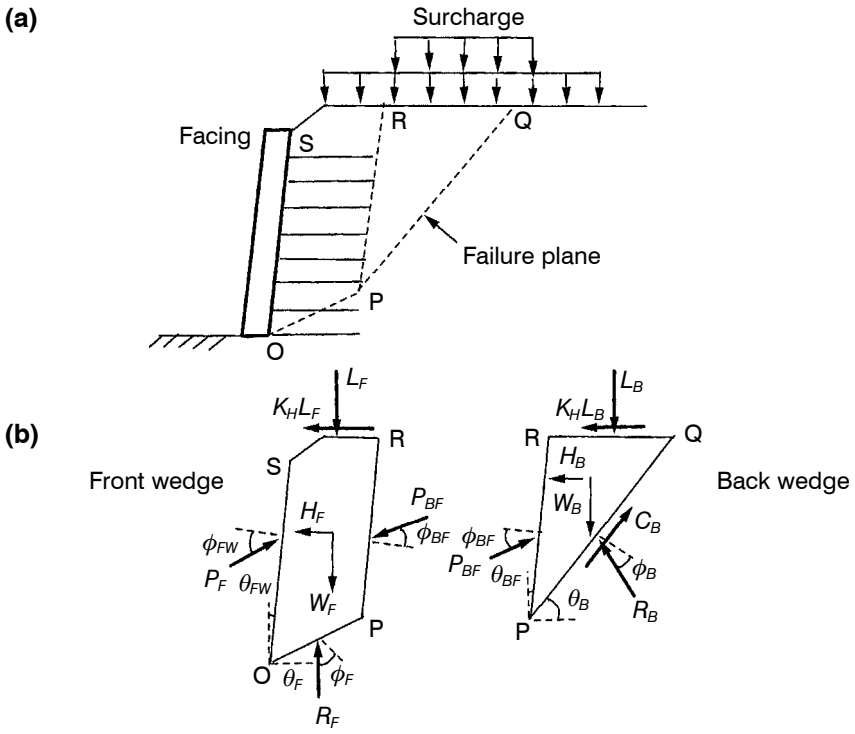

Figure 9. Two wedge method for a reinforced soil-type wall (after Horii et al. 1994): (a) cross section; (b) force diagram.

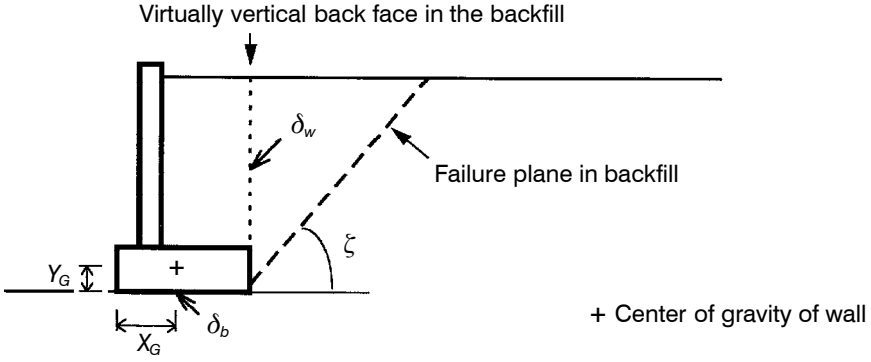

Figure 10. Definition of the failure plane angle, ζ, and the parameters used in Table 3 for the model cantilever-type wall.

Considering the effect of the sand paper glued on the surface of the wall base, the interface friction angle, δ_b , between the subsoil and the wall base, which was used to calculate factors of safety against sliding, was assumed to equal 3/4ϕ (38°). The ratio of 3/4 is equal to the ratio of the angle of friction on the horizontal failure plane obtained from simple shear tests, $\phi_{ss} = \arctan(\tau/\sigma_n)_{max}$, to the angle of friction obtained from plane strain compression tests, $\phi_{psc} = \arcsin\{(\sigma_1 - \sigma_3)/(\sigma_1 + \sigma_3)_{max}\}$ (where σ_3 is the minor principal stress), with a vertical σ_1 direction. Both ϕ_{ss} and ϕ_{psc} were obtained for air-pluviated Toyoura sand (Figure 11) (Tatsuoka et al. 1991). It is likely that δ_b is equivalent to the simple shear angle of friction, ϕ_{ss} . Similarly, by neglecting the effect of anisotropy, the interface friction angle, δ_w , between the backfill and the wall facing with sand paper or along the aforementioned virtually vertical back face within the backfill, was also assumed to equal 3/4ϕ. Table 3 summarizes the parameters used for the stability analysis.

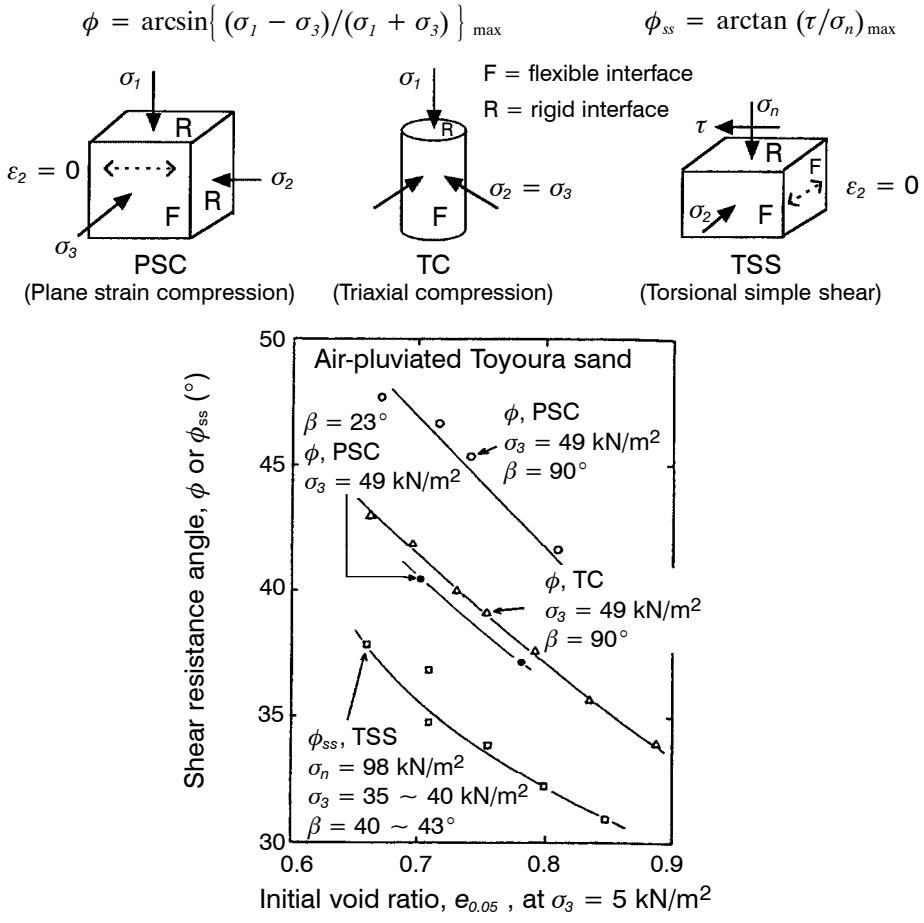

Figure 11. Comparison of the shear resistance angles, ϕ or ϕ_{ss} , of air-pluviated Toyoura sand (after Tatsuoka et al. 1991).

Note: β = angle of σ_1 direction relative to the direction of the bedding plane.

Table 3. The parameters used for the prediction of wall stability.

Physical property	Type of model wall			
	Cantilever	Gravity	Leaning	Reinforced soil
Mass per unit length, m (kg/m)	34.1	159.0	84.6	19.8
Location of center of gravity, X_G , Y_G (m)*	0.089, 0.177	0.101, 0.142	0.149, 0.166	0.015, 0.250
Dry unit weight of the backfill and subsoil, ϱ (kN/m^3)	15.9	15.9	15.9	15.9
Shear resistance angle of the backfill and subsoil, ϕ (°)**	51	51	51	51
Interface friction angle between the wall bottom and subsoil, δ_b (°)	38 (= 3/4ϕ)	38 (= 3/4ϕ)	38 (= 3/4ϕ)	38 (= 3/4ϕ)
Interface friction angle between the wall bottom or along the virtual vertical back face in the backfill and wall facing, δ_w (°)***	38 (= 3/4ϕ)	38 (= 3/4ϕ)	38 (= 3/4ϕ)	38 (= 3/4ϕ)

Notes: * Refer to Figure 10 for the definition of X_G , Y_G and the virtually vertical back face in the backfill. ** No cohesion was assumed. *** For reinforced-soil retaining model walls, ϕ_{FW} and ϕ_{BF} in Figure 9 were set equal to δ_w .

The horizontal seismic coefficient, k_h , used in the pseudo-static stability analysis approach was evaluated as follows for shaking table and tilt table tests, respectively:

$$k_h = \alpha / g \tag{1}$$

$$k_h = \tan\theta \tag{2}$$

where: α = amplitude of the base horizontal acceleration; θ = tilting angle of the sand box; and g = gravitational acceleration. Dynamic effects in the shaking table tests, such as amplification and phase difference of the response acceleration in the model, were not considered in the evaluation of model wall stability.

Typical results of the stability analysis are shown in Figures 12 and 13 for the cantilever-type wall and the reinforced soil, Type 1 model walls, respectively, where the predicted values for different interface friction angles, $\delta = \delta_b = \delta_w$, set equal to $1/2\phi$ and ϕ are also shown. Effects of the interface friction angle were significant in determining the factors of safety against sliding for model walls other than the reinforced soil-type, because these factors of safety are directly affected by the interface friction angle, δ_b , between the subsoil and the wall base. The critical seismic acceleration coefficients against overturning, yielding a factor of safety of unity, were also sensitive to the interface friction angle because a relatively large increase in the seismic coefficient was required to reduce the factors of safety against overturning when the factors of safety approached unity (Figure 12).

It is noted that for all types of model walls, the effect of progressive failure of the backfill was not considered in the stability analysis. That is, the peak friction angle, ϕ, which was equal to 51° in this case, may not be simultaneously mobilized along the failure plane, but the operating average angle may be smaller, and the ratio of the peak and operating angles may depend on the failure mode and the wall type. Further discussion of this point is beyond the scope of the current paper.

It is also noted that the interface friction angle activated along the virtually vertical back face within the backfill for the cantilever-type and reinforced soil-type model

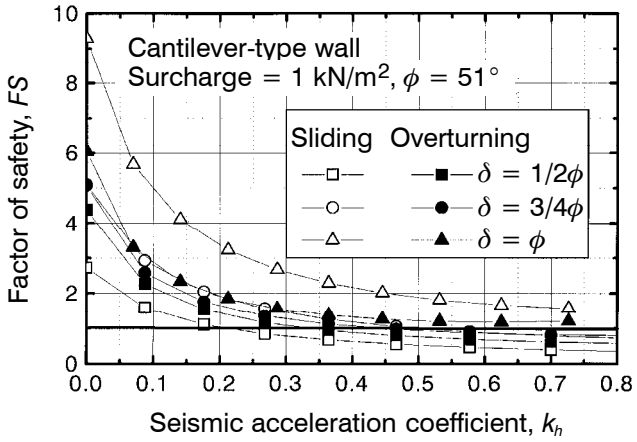

Figure 12. Predicted factors of safety for a model cantilever-type retaining wall during shaking table tests.

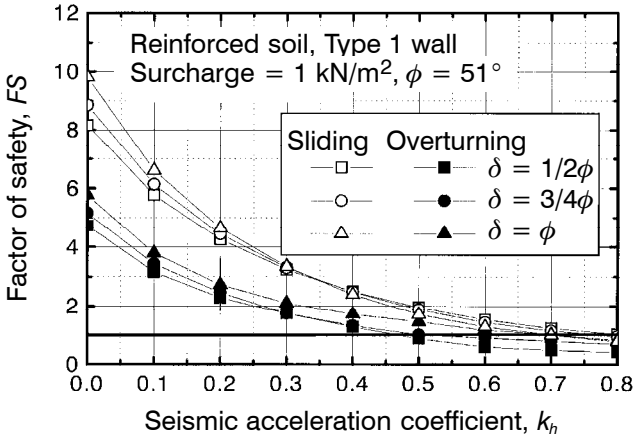

Figure 13. Predicted factors of safety for a model reinforced soil, Type 1 retaining wall during shaking table tests.

walls may be larger than that activated at the interface between the backfill and the wall facing for the gravity-type and the leaning-type model walls. This point will be discussed in Section 4.1.

Furthermore, in the present stability analysis against overturning, the center of rotation was assumed to be located at the toe of the wall base. For the cantilever-type, gravity-type, and leaning-type walls, however, the center of rotation moved backwards when the bearing capacity in the subsoil below the facing was lost during shaking/tilting. On the other hand, for the reinforced soil-type retaining walls, due to the flexibility of the backfill, the stress transfer from the facing bottom back into the bottom of the reinforced zone was less than that for the cantilever-type, gravity-type, and leaning-type walls.

This resulted in less backward movement of the center of rotation and less reduction in the stability against overturning.

4 RESULTS AND DISCUSSIONS

4.1 Model Wall Stability in the Shaking Table Tests

For all of the models, the major failure mode of the walls was overturning as shown in Figure 1. It is seen from Figure 6 that the outward displacement measured by displacement transducer D1 near the bottom of the reinforced soil, Type 1 wall facing, was much smaller than that near the top of the facing measured by displacement transducer, D3. This indicates that the transitional component of the facing displacement was much smaller than its rotational component. It should be also noted that the subsoil immediately in front of the facing suffered a slight heaving, as measured by displacement transducer D4, which is possibly due to the occurrence of bearing capacity failure in the subsoil below the facing.

In order to compare the relative stability of different wall types, the observed critical accelerations were defined as the amplitude of the base acceleration (measured by accelerometer A11 in Figure 6) in the active state (corresponding to negative acceleration values in Figure 6) when the outward displacement at the top of the facing reached 5% of the total wall height (approximately 25 mm). Note that, after the outward displacement at the top of the facing exceeded 5% of the total wall height, the displacement began to increase in an uncontrollable manner as was typically demonstrated by displacement transducer D3 in Figure 6.

In Figure 14, the observed critical seismic acceleration coefficients, $k_{h\text{-}cr(obs)}$, are compared with the predicted critical seismic acceleration coefficients, $k_{h\text{-}cr(cal)}$, which resulted in a factor of safety of unity against overturning for $\delta = 3/4\phi$. For this comparison, accelerations (see Table 1 for the observed critical accelerations) were converted to seismic coefficients by using Equation 1.

For the cantilever-type, leaning-type, and gravity-type model walls, the observed values were almost equal to or smaller than the predicted values against overturning. The relative difference was larger in the order of the gravity-type, leaning-type, and cantilever-type walls. The smaller observed critical seismic coefficient for the gravity-type and leaning-type walls may be related to the inference that, as mentioned in Section 3, the interface friction angle δ_w activated between the backfill and the wall facing was smaller than the interface friction angle activated along the virtually vertical back face within the backfill of the cantilever-type wall. On the other hand, the observed value was slightly larger than the predicted value for the reinforced soil, Type 1 model wall, and noticeably larger for the reinforced soil, Type 2 model wall.

The larger observed critical seismic coefficients for the reinforced-soil walls may be due to the difference in the location of center of rotation (Section 3); i.e. the center of rotation moves away from the wall face into the backfill after the bearing capacity failure of the subsoil below the facing in the case of the gravity-type, leaning-type, and cantilever-type walls. The distance of the same point of rotation from the back of the wall is less in the case of the reinforced soil walls due to the flexibility of the backfill.

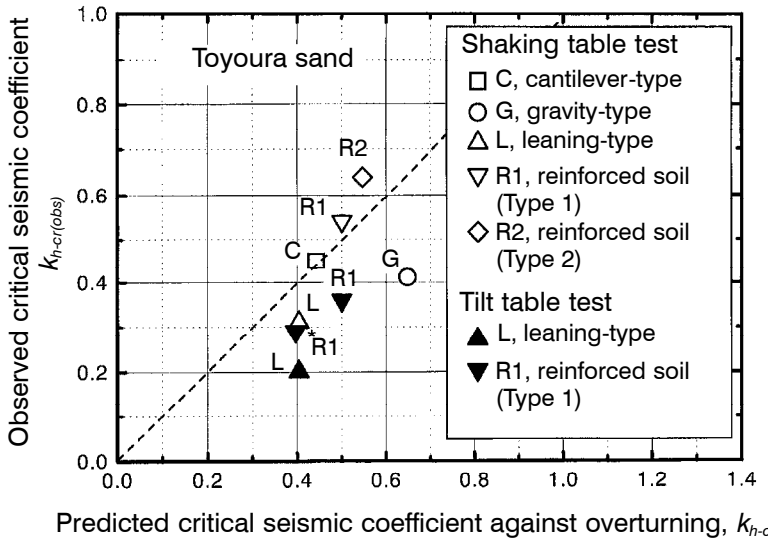

Figure 14. Comparison of the observed critical seismic coefficients, $k_{h\text{-}cr(obs)}$, to the predicted critical seismic coefficients, $k_{h\text{-}cr(cal)}$, against overturning, assuming $\delta = 3/4\phi$.
Note: * Surcharge of 3.1 kPa; 1.0 kPa surcharge used in all of the other tests.

It may also be seen from Figure 14 that the observed critical seismic coefficients for the different model walls scatter over a large range, while the corresponding values predicted by the pseudo-static stability analysis are within a relatively narrow range. This result indicates that the pseudo-static stability analysis cannot evaluate important aspects of the seismic stability of different types of walls. Particularly, the stability of the reinforced soil-type model walls in the shaking table test is underestimated by the current pseudo-static stability analysis in comparison with the gravity- and leaning-type retaining walls.

In Figure 15, the observed critical seismic coefficients, $k_{h\text{-}cr(obs)}$, are compared to the predicted coefficients, $k_{h\text{-}cr(cal)}$, against sliding for all of the models for $\delta = 3/4\phi$. It may be seen that the predicted values, $k_{h\text{-}cr(cal)}$ against sliding for all of the model walls were larger than the observed values, $k_{h\text{-}cr(obs)}$, which is consistent with the fact that the observed failure mode in all of the tests was overturning. However, these predicted values are not very reliable, because the values are too sensitive to the interface friction angle of the model walls except for the reinforced soil-type (Figure 13).

It is to be noted that for the reinforced soil-type model walls, although the reinforced backfill was assumed to behave as a rigid body when the factors of safety were evaluated, during the tests overturning of the wall accompanied simple shear deformation of the reinforced backfill (Figures 1d and 1e). This behavior suggests that the horizontally placed reinforcement layers do not effectively resist such simple shear deformation of the reinforced backfill. In evaluating seismically induced residual displacement of geosynthetic-reinforced soil retaining walls, therefore, simple shear deformation of the reinforced backfill should be taken into account as stated by Tatsuoka et al. (1996a).

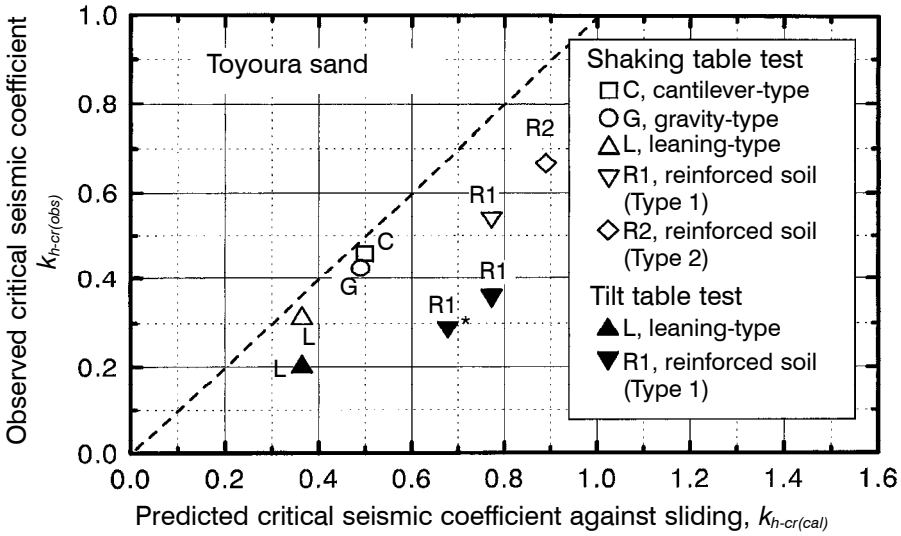

Figure 15. Comparison of the observed critical seismic coefficients, $k_{h\text{-}cr(obs)}$, to the predicted critical seismic coefficients, $k_{h\text{-}cr(cal)}$, against sliding assuming $\delta = 3/4\phi$.

Note: * Surcharge of 3.1 kPa; 1.0 kPa surcharge used in the other tests.

4.2 Model Wall Stability in the Tilt Table Tests

In Figure 14, the observed critical tilting angles that caused outward displacements at the facing top as large as 5% of the total wall height are also compared with the predicted critical tilting angles which resulted in a factor of safety of unity against overturning. The tilting angles were converted to seismic coefficients by using Equation 2. For the same model wall type with the same surcharge, the predicted critical seismic coefficients for shaking and tilt table tests are the same according to the pseudo-static analysis.

For the same wall type, however, the observed critical seismic coefficient is smaller for the tilt table tests than for the shaking table tests (Figure 14). This may have been caused by an essential difference in the testing conditions; i.e. the seismic horizontal force was simulated pseudo-statically in tilt table tests, while it was applied periodically for approximately ten seconds in the shaking table tests. For the same seismic coefficient, the loading condition was more severe with respect to wall stability for the tilt table tests than the shaking table tests; however, the opposite was true when the effects of amplification were large in the shaking table tests. It seems that for the test cases presented in the current paper, the effects of the former factor are more predominant than the latter factor.

Analyses of the recorded data, on the effects of amplification and phase difference in the response acceleration during shaking, are in progress. These analyses will be extended to the effects of frequency and irregularity of the actual earthquake motion for practical applications.

4.3 Angle of the Failure Plane

The failure plane in the backfill was observed in the central wall cross section during removal of the models after the tests and was nearly straight for all of the models except the reinforced soil, Type 2 model wall (Figure 1e). The angle of the lower section of the observed failure planes measured from the horizontal are listed in Tables 1 and 2. In Figure 16, the relationships between the observed critical seismic coefficients, $k_{h\text{-}cr(obs)}$, and the observed failure plane angle, ζ, are compared with the predicted critical seismic coefficients and the predicted failure plane angle based on the Mononobe-Okabe method.

For the Mononobe-Okabe method, the same assumptions were made as in the prediction of wall stability (Section 3). For the reinforced soil, Type 2 model wall, there were multiple failure planes (Figure 1e). Failure plane 1 starts at the heel of the backfill zone that was reinforced with short reinforcement layers and stops below the lower long reinforcement, while failure plane 2 and 3, which are significantly closer to the horizontal, extend to the crest of the backfill. It is likely that failure plane 1 and 2 developed first and second, respectively, and that these failure planes were initially at an angle similar to failure planes observed in the other models. However, due to the shear deformation of the reinforced backfill (Section 4.1), which occurred after the appearance of these failure planes until the end of the tests, the angle of the failure plane, ζ, increased. These failure planes will not be discussed herein, because the angle of the failure planes at the moment of appearance have not yet been estimated.

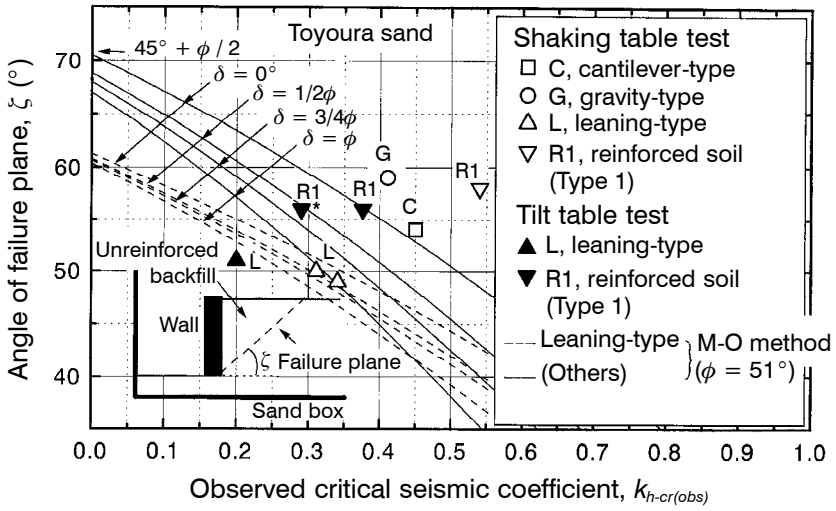

Figure 16. Relationships between the observed critical seismic coefficients, $k_{h\text{-}cr(obs)}$, and the observed angle of the failure plane, ζ, and the predicted relationship calculated using the Mononobe-Okabe method.

Note: * Surcharge of 3.1 kPa; 1.0 kPa surcharge used in the other tests.

To predict the failure plane, it was assumed that $\delta_w = 3/4\phi$. The failure planes observed for the cantilever-type, gravity-type, and reinforced soil, Type 1 model walls in the shaking table tests, and the failure planes for the reinforced soil, Type 1 model walls with a surcharge of 1.0 kN/m^2 in the tilt table tests were steeper than the predicted failure planes. For the shaking table tests, the difference was greater for the reinforced soil, Type 1 model wall than for the cantilever- and gravity-type model walls. Also, for the tilt table tests on the reinforced soil, Type 1 model wall with a larger surcharge, the observed failure plane was steeper than the predicted failure plane, although the difference is marginal.

It should be noted that the predicted failure plane angle decreases as the seismic coefficient increases (Figure 16). On the other hand, the shaking acceleration or the tilting angle could be increased further, even after slight movement of the wall, without causing an abrupt ultimate failure. The failure plane developed further during the increase of shaking acceleration/tilting angle, as typically seen from Figure 5 for the reinforced soil, Type 1 model wall. It is important to note, however, that no multiple failure planes in the backfill were observed in the models, except for the reinforced soil, Type 2 model wall.

The active earth pressure coefficient, K_a , was calculated for $\delta_w = 3/4\phi$ by the trial wedge method assuming a vertical interface between the backfill and the wall. In Figure 17, the results are plotted versus the angle of the direction of the bottom failure plane of the trial wedge, ζ. For simplicity, the seismic coefficient k_h was set to 0, 0.2, and 0.4 in Cases 1, 2, and 3, respectively. In these cases, the shear resistance angle ϕ was set to 51°, which corresponds to the peak resistance of the backfill, as was the case with the aforementioned prediction of wall stability (Section 3). On the other hand, for Case 4, the value of ϕ was reduced to 34°, which approximately corresponds to the residual angle of friction, ϕ_{res} , while keeping $k_h = 0.4$. Similarly, the value of δ for Cases 3 and 4 was reduced to 29° by assuming the residual condition for this interface friction angle

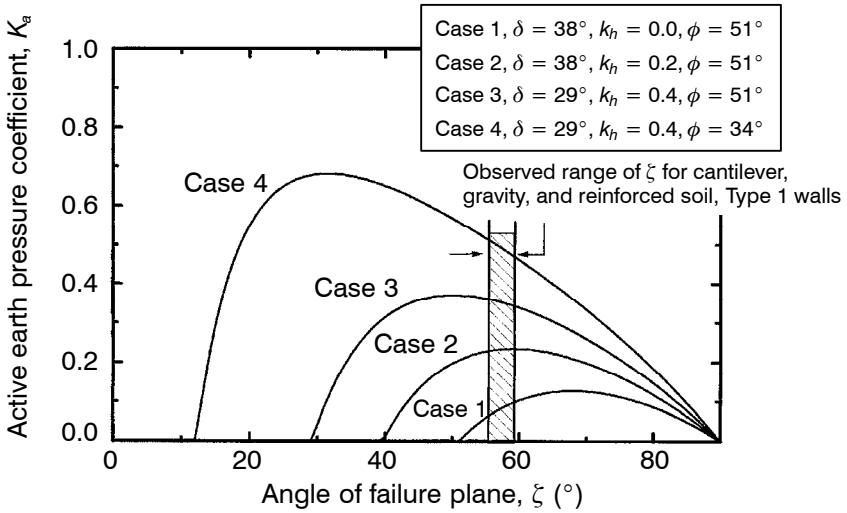

Figure 17. Relationships between the angle of failure plane, ζ, and the coefficient of active earth pressure, K_a .

($[\phi_{ss}]_{res}$ = arctan{sin[ϕ_{ss}]}). The range of failure plane angles observed for the cantilever-type, gravity-type, and reinforced soil, Type 1 model walls during shaking are also shown in Figure 17. Based on Figure 17, the formation of a single failure plane during shaking may be outlined in the following steps:

1. Before shaking, it was not necessary to mobilize the peak shear resistance at the bottom of the trial wedge because the wall was relatively stable. The earth pressure acting on the wall was, therefore, between the "at rest" earth pressure and the active earth pressure obtained by using the maximum value of K_a for Case 1.
2. During shaking, the relative stability of the wall was gradually lowered with the increase in shaking acceleration. For example, at an equivalent seismic coefficient k_h = 0.2 for Case 2, the peak shear resistance at the bottom of the trial wedge was mobilized, and the failure plane was formed at an angle which yielded the maximum value of K_a.
3. As the shaking acceleration increased further, the shear resistance along the failure plane formed in Step 2 was reduced to its residual value due to displacements along the failure plane, while its peak value was still maintained along other potential failure planes. For example, when k_h = 0.4 the value of K_a for Case 4, for the range of observed failure plane angles, was larger than the maximum value of K_a for Case 3. Therefore, sliding of the soil wedge, along the previously formed failure plane with ζ = 55 to 59°, was mobilized without changing the angle of the failure plane. This mechanism would also explain why the observed failure plane was steeper than the predicted failure plane (ζ = 48° for Case 3) that was obtained by assuming that the peak shear resistance can always be mobilized uniformly in the backfill.

For the leaning-type model walls, the angle of the failure plane observed in the shaking table tests was almost equal to or slightly larger than the predicted value, while it was even smaller in the tilt table test. This was due to the fact that the leaning-type model walls failed relatively abruptly during shaking after the appearance of the failure plane, when compared to the behavior of the other types of walls.

In order to clarify and compare the failure mechanism of retaining walls of different types, analyses based on the recorded earth pressures, wall displacements, and response accelerations are necessary. These analyses are now in progress and will be reported in the future.

5 CONCLUSIONS

For the shaking table tests performed in the current study, the major observed failure mode was overturning with tilting of the wall face, which may have been triggered by a bearing capacity failure in the subsoil below the wall facing. The observed critical seismic acceleration coefficients were equal to or smaller than the predicted values against overturning for the cantilever-, gravity-, and leaning-type model walls. On the other hand, the observed critical seismic acceleration coefficient was slightly larger than the predicted value for the reinforced soil, Type 1 model wall with reinforcement of equal length. Also, the ratio of the observed to predicted critical seismic acceleration coefficients was much larger for the reinforced soil, Type 2 model wall which had longer reinforcement at higher wall levels.

These results suggest that ordinary pseudo-static seismic stability analyses based on the limit equilibrium method, used for the prediction of the critical seismic acceleration coefficients in the current study, underestimate the seismic stability of reinforced soil retaining walls in comparison with conventional, gravity-type soil retaining walls. These results are consistent with the observations of the seismic behaviour of reinforced soil retaining walls, conventional, reinforced concrete cantilever retaining walls, and conventional, gravity-type retaining walls during the 1995 Hyogoken-Nanbu Earthquake described in Section 1. These results also show that the long reinforcement layers placed at higher levels in the backfill can substantially increase the resistance against overturning failure. However, this contribution is not properly evaluated by the conventional stability analysis mentioned above.

The residual deformation of these reinforced soil-type walls accompanied simple shear deformation along horizontal planes in the reinforced backfill, which should be considered in evaluating seismically induced residual deformation of geosynthetic-reinforced soil retaining walls.

The relative stability of the same wall type was quantitatively lower in the tilt table tests than in the shaking table tests. This may have been caused by the essential difference in the testing conditions whether the seismic horizontal force was simulated pseudo-statically or dynamically.

For the cantilever-type, gravity-type, and the reinforced soil, Type 1 model walls, the failure plane angle in the backfill observed in the central cross section after the shaking table tests was steeper than the predicted angle. The difference was larger for the reinforced soil, Type 1 model wall than for the cantilever-type and gravity-type model walls. The difference between the predicted and observed failure plane angles were smaller for the tilt table tests.

Multiple failure planes in the backfill were not observed in the cantilever-type, gravity-type, and the reinforced soil, Type 1 model walls after the shaking table tests, despite the increase of the shaking acceleration and tilting angle after the appearance of the failure plane which did not cause ultimate failure. This behavior may be explained by considering the post-peak reduction of shear resistance along the previously formed failure plane from its peak value to its residual value. The behavior of the leaning-type model walls during shaking may also be qualitatively explained by considering their abrupt failure.

REFERENCES

Bathurst, R.J. and Alfaro, M.C., 1996, "Review of Seismic Design, Analysis and Performance of Geosynthetic Reinforced Walls, Slopes and Embankments", *Earth Reinforcement*, Ochiai, H., Yasufuku, N. and Omine, K., Editors, Balkema, Vol. 2, Proceedings of International Symposium on Earth Reinforcement, Fukuoka, Kyushu, Japan, November 1996, Keynote Lecture, pp. 887-918.

Bathurst, R.J. and Cai, Z., 1995, "Pseudo-Static Seismic Analysis of Geosynthetic-Reinforced Segmental Walls", *Geosynthetics International*, Vol. 2, No. 5, pp. 787-830.

Horii, K., Kishida, H., Tateyama, M. and Tatsuoka, F., 1994, "Computerized Design Method for Geosynthetic-Reinforced Soil Retaining Walls for Railway Embankments", *Recent Case Histories of Permanent Geosynthetic-Reinforced Soil Retaining Walls*, Tatsuoka, F. and Leshchinsky, D., Editors, Balkema, Proceedings of Seiken Symposium No. 11, Tokyo, Japan, November 1992, pp. 205-218.

Koseki, J., Tateyama, M., Tatsuoka, F. and Horii, K., 1996, "Back Analyses of Soil Retaining Walls for Railway Embankments Damaged by the 1995 Hyogoken-Nanbu Earthquake", *The 1995 Hyogoken-nanbu Earthquake - Investigation into Damage to Civil Engineering Structures*, Committee of Earthquake Engineering, Japan Society of Civil Engineers, pp. 101-114.

Murata, O., Tateyama, M. and Tatsuoka, F., 1992, "Loading Tests of Geosynthetic-Reinforced Soil Retaining Walls and Their Stability Analyses", *Earth Reinforcement Practice*, Ochiai, H., Hayashi, S. and Otani, J., Editors, Balkema, Vol. 1, Proceedings of International Symposium on Earth Reinforcement Practice, Fukuoka, Kyushu, Japan, November 1992, pp. 385-390.

Murata, O., Tateyama, M. and Tatsuoka, F., 1994, "Shaking Table Tests on a Large Geosynthetic-Reinforced Soil Retaining Wall Model", *Recent Case Histories of Permanent Geosynthetic-Reinforced Soil Retaining Walls*, Tatsuoka, F. and Leshchinsky, D., Editors, Balkema, 1994, Proceedings of Seiken Symposium No. 11, Tokyo, Japan, November 1992, pp. 259-264.

Sakaguchi, M. 1996, "A Study of the Seismic Behavior of Geosynthetic Reinforced Walls in Japan", *Geosynthetics International*, Vol. 3, No. 1, pp. 13-30.

Tatsuoka, F., Okahara, M., Tanaka, T., Tani, K., Morimoto, T. and Siddiquee, M.S.A., 1991, "Progressive Failure and Particle Size Effect in Bearing Capacity of a Footing on Sand", *Geotechnical Engineering Congress 1991*, McLean, F., Campbell, D.A. and Harris, D.W., Editors, ASCE, Geotechnical Special Publication No. 27, Vol. 2, Proceedings of a congress held in Boulder, Colorado, USA, June 1991, pp. 788-802.

Tatsuoka, F., Tateyama, M. and Murata, O., 1989, "Earth Retaining Wall with a Short Geotextile and a Rigid Facing", *Proceedings of the Twelfth International Conference on Soil Mechanics and Foundation Engineering*, Balkema, 1992, Vol. 2, Rio de Janeiro, Brazil, August 1989, pp. 1311-1314.

Tatsuoka, F., Koseki, J. and Tateyama, M., 1996a, "Performance of Reinforced Soil Structures during the 1995 Hyogo-ken Nanbu Earthquake", *Earth Reinforcement*, Ochiai, H., Yasufuku, N. and Omine, K., Editors, Balkema, Vol. 2, Proceedings of International Symposium on Earth Reinforcement, Fukuoka, Kyushu, Japan, November 1996, Special Report, pp. 973-1008.

Tatsuoka, F., Tateyama, M. and Koseki, J., 1996b, "Performance of Soil Retaining Walls for Railway Embankments", *Soils and Foundations*, Special Issue of Soils and Foundations on Geotechnical Aspects of the January 17 1995 Hyogoken-Nambu Earthquake, pp. 311-324.

Tatsuoka, F., Tateyama, M., Uchimura, T. and Koseki, J., 1997, "Geosynthetics-Reinforced Soil Retaining Walls as Important Permanent Structures, Mercer Lecture 1996-1997", *Geosynthetics International*, Vol. 4, No. 2, pp. 81-136.

NOTATIONS

Basic SI units are given in parentheses.

C_B = sliding resistance due to cohesion of backfill, back wedge (Figure 9) (N/m)
d_{50} = mean particle diameter (m)
EI = bending stiffness (N-m^2)
e_{max} = maximum void ratio of backfill and subsoil sand (dimensionless)
e_{min} = minimum void ratio of backfill and subsoil sand (dimensionless)
FS = factor of safety (dimensionless)
g = acceleration due to gravity (m/s^2)
H_B = inertia force due to horizontal seismic load acting on back wedge (Figure 9) (N/m)
H_F = inertia force due to horizontal seismic load acting on front wedge (Figure 9) (N/m)
K_H = horizontal seismic coefficient to evaluate inertia force of surcharge (Figure 9) (N/m)
K_a = active earth pressure coefficient (dimensionless)
k_h = horizontal seismic coefficient to evaluate inertia force of facing and backfill (dimensionless)
$k_{h\text{-}cr}$ = critical seismic coefficient (dimensionless)
$k_{h\text{-}cr(cal)}$ = predicted critical seismic coefficient (dimensionless)
$k_{h\text{-}cr(obs)}$ = observed critical seismic coefficient (dimensionless)
L_B = vertical force due to surcharge acting on back wedge (Figure 9) (N/m)
L_F = vertical force due to surcharge acting on front wedge (Figure 9) (N/m)
m = mass per unit length of model wall (kg/m)
P_{BF} = interwedge force (Figure 9) (N/m)
P_F = reactive force at interface between front wedge and facing (Figure 9) (N/m)
$PHGA$ = peak horizontal ground acceleration (m/s^2)
R_B = reactive force at bottom of back wedge (N/m)
R_F = reactive force at bottom of front wedge (N/m)
W_B = weight of back wedge (N/m)
W_F = weight of front wedge (N/m)
X_G = x-coordinate of center of gravity of model (Figure 10) (m)
Y_G = y-coordinate of center of gravity of model (Figure 10) (m)
α = amplitude of base horizontal acceleration (m/s^2)
β = angle of σ_1 direction relative to bedding plane (°)
δ = interface friction angle (°)

δ_b = interface friction angle between subsoil and wall base (°)
δ_w = interface friction angle between backfill and wall facing (°)
ε_2 = intermediate principle strain (Figure 11) (dimensionless)
ϕ = shear resistance angle of soil (°)
ϕ_B = shear resistance angle mobilized at bottom of back wedge (Figure 9) (°)
ϕ_{BF} = interwedge shear resistance angle (Figure 9) (°)
ϕ_F = shear resistance angle mobilized at front of back wedge (Figure 9) (°)
ϕ_{FW} = shear resistance angle mobilized at interface between front wedge and facing (Figure 9) (°)
ϕ_{psc} = shear resistance angle from plane strain compression tests having the vertical σ_1 direction (°)
ϕ_{res} = shear resistance angle at residual state (°)
ϕ_{ss} = shear resistance angle mobilized on horizontal failure plane from simple shear tests (°)
θ = tilting angle of sand box (°)
θ_B = angle of bottom plane of back wedge measured from horizontal (Figure 9) (°)
θ_{BF} = angle of interwedge plane measured from vertical (Figure 9) (°)
θ_F = angle of bottom plane of front wedge measured from horizontal (Figure 9) (°)
θ_{FW} = angle of back-face of facing measured from vertical (Figure 9) (°)
ϱ = dry unit weight of backfill and subsoil sand (N/m^3)
σ_n = normal stress (Figure 11) (N/m^2)
σ_1 = major principal stress (N/m^2)
σ_2 = intermediate principle stress (Figure 11) (N/m^2)
σ_3 = minor principal stress (N/m^2)
τ = shear stress (N/m^2)
ζ = angle of failure plane measured from horizontal (°)

Erratum

SHAKING AND TILT TABLE TESTS OF GEOSYNTHETIC-REINFORCED SOIL AND CONVENTIONAL-TYPE RETAINING WALLS

TECHNICAL PAPER FOR ERRATUM: Koseki, J., Munaf, Y., Tatsuoka, F., Tateyama, M., Kojima, K. and Sato, T., 1997, "Shaking and Tilt Table Tests of Geosynthetic-Reinforced Soil and Conventional-Type Retaining Walls", *Geosynthetics International*, Vol. 5, Nos. 1-2, pp. 73-96.

PUBLICATION: *Geosynthetics International* is published by the Industrial Fabrics Association International, 1801 County Road B West, Roseville, Minnesota 55113-4061, USA, Telephone: 1/651-222-2508, Telefax: 1/651-631-9334. *Geosynthetics International* is registered under ISSN 1072-6349.

REFERENCE FOR ERRATUM: Koseki, J., Munaf, Y., Tatsuoka, F., Tateyama, M., Kojima, K. and Sato, T., 1999, "Errata for 'Shaking and Tilt Table Tests of Geosynthetic-Reinforced Soil and Conventional-Type Retaining Walls'", *Geosynthetics International*, Vol. 6, No. 6, p. 519.

The Editors regret the errors incurred in Figures 7a, 7b, and 7c, Section 2.3, p. 81, during type-setting of the authors paper, which appeared in *Geosynthetics International*, Vol. 5, Nos. 1-2.

ERRATUM FOR SECTION: 2.3 Tilt Table Tests

In Figures 7a, 7b, and 7c, p. 81 :

The *y*-axes units should be force in newtons (N) and not kilonewtons (kN).